Chemical Engineering Journal 348 (2018) 212–223

Contents lists available at ScienceDirect

Chemical Engineering Journal

journal homepage: www.elsevier.com/locate/cej

Efficiently texturing hierarchical epoxy layer for smart superhydrophobic surfaces with excellent durability and exceptional stability exposed to fire

Shanshan Jia[a], Xihong Lu[b], Sha Luo[a], Yan Qing[a,c,*], Ning Yan[d], Yiqiang Wu[a,c,*]

[a] College of Materials Science and Engineering, Central South University of Forestry and Technology, Changsha 410004, PR China
[b] School of Chemistry, Sun Yat-Sen University, Guangzhou 510275, PR China
[c] Hunan Provincial Collaborative Innovation Center for High-efficiency Utilization of Wood and Bamboo Resources, Central South University of Forestry and Technology, Changsha 410004, PR China
[d] Faculty of Forestry, University of Toronto, Toronto M5S3B3, Canada

HIGHLIGHTS

- We develop a novel method to texture hierarchical adhesive coating.
- The adhesive coating with WCA of ~156° shows great superhydrophobicity.
- The coating can apply on various substrates to obtain superhydrophobic surface.
- Superhydrophobic surface shows excellent mechanical robustness.
- Superhydrophobic surface shows exceptional stability exposed to fire.

ARTICLE INFO

Keywords:
Superhydrophobic surfaces
Thermally driven strategy
Hierarchical epoxy layer
Mechanical durability
Stability exposed to fire

ABSTRACT

Coating superhydrophobic protective layers onto the lignocellulosic materials is promising to endow them with multifunctions, including waterproof, flame retardance, etc. However, appropriate approaches capable of engineering durable superhydrophobic lignocellulosic materials are still lacking. In this work, we developed an efficient thermally driven strategy to prepare durable superhydrophobic surfaces without the need for complicated pre/post treatment by immersing the lignocellulosic materials into a sealed vessel with a mixture of massive epoxy and SiO_2 nanoparticles (NPs). The hierarchical structure was induced by the epoxy layer with micrometer-sized pores and the incompletely enclosure of SiO_2 NPs. The unique hierarchical structure contributes to the superhydrophobic surfaces with a remarkable contact angle of 156° and sliding angle of 2°. Such prepared water repellent surfaces exhibited excellent durability when are subjected to mechanical abrasion, chemical corrosion, and harsh environmental conditions. In particular, the functional surfaces retained their original superhydrophobicity even when directly exposed to fire for 50 s. These surfaces fabricated on lignocellulose-based materials displayed exceptional flame retardancy manifested by a significant improvement in ignition delay. The superhydrophobic surfaces with impressive mechanical stability, superior thermal stability, and flame retardancy hold substantial potentials for practical applications in a broad range of fields.

1. Introduction

Lignocellulose, as an important kind of renewable and environmentally friendly biopolymer, has been extensively used throughout the human history [1–4]. The major problems of lignocellulose-based manufactures are that they tend to start rotting when exposed to high humidity environment or water and are prone to get fire [5,6]. One possible approach to solve these problems is to coat the surface of these manufactures with a multifunctional (e.g., waterproof and flame-retardant) layer. Extensive studies have been devoted to engineer superhydrophobic surfaces encouraged by the outstanding water-repellent performance of lotus leaves [5,7–9]. Besides the waterproof property, these superhydrophobic coatings endow a variety of interesting functions to the substrate materials, such as self-cleaning [10–13], drag reduction [14,15], selective absorption [16–19], anti-icing [20–24], anti-corrosion [25,26], and anti-fogging [27]. However, the textural fragility of the superhydrophobic coating and the poor affinity between the coating and the lignocellulose render a short

* Corresponding authors at: College of Materials Science and Engineering, Central South University of Forestry and Technology, Changsha 410004, PR China.
E-mail addresses: qingyan0429@163.com (Y. Qing), wuyq0506@126.com (Y. Wu).

https://doi.org/10.1016/j.cej.2018.04.195
Received 24 February 2018; Received in revised form 19 April 2018; Accepted 27 April 2018
Available online 30 April 2018
1385-8947/

longevity of the superhydrophobic materials [28–34].

Self-healing superhydrophobic coatings that can restore the physical damage of the coatings have been adopted to improve the durability of the superhydrophobic coatings on the lignocellulose-based materials [35–41]. However, the complex self-healing procedures (e.g., ultraviolet exposure, heating treating, etc.) and the limited healing times make this approach unrealistic. Inserting a binding layer between lignocellulose and the superhydrophobic coatings seems promising to generate durable superhydrophobic lignocellulose-based materials [34,42–49]. However, this kind of coatings are still not strong enough and will be ruptured under extreme abrasion, because the functional NPs in support of superhydrophobicity were only arranged on the surface of the adhesive layer . Coating the lignocellulose-based materials with a mixture of adhesive glues and nanoparticles can form a strong anti-wear layer, but with poor hydrophobic performance owing to the smooth surface. Roughening the surface has been achieved using different approaches, such as plasma treatment, immersing into the corrosive liquid, and heat etching [50–52]. These treatments, however, will inevitably influence the intrinsic property of lignocellulose. Moreover, such prepared coatings still have unsatisfactory superhydrophobic properties, especially in high temperature environments. Therefore, a simple approach that can prepare superhydrophobic coatings with strong adhesion to lignocellulose, a good durability, as well as flame retardance is still highly desirable.

Here, we developed an approach to prepare superhydrophobic coatings with excellent durability and exceptional stability even exposed to fire. The functionalized coating was readily obtained by a one-step thermally-driven method using a solution consisting of epoxy, SiO_2 nanoparticles (NPs), perfluorooctyltrimethoxysilane (F13-TMS), and ethanol. This one-step thermally-driven method includes two stages: solution immersion and evaporation. The initial solution immersion process allows ethanol to penetrate into the substrate where the epoxy layer is deposited beneath the NPs under different settling velocity effect. Micropores are created in the epoxy layer by the impact force from the release of gaseous ethanol during the following evaporation process. The two processes yield a hierarchically structured composite coating, with a sufficient bonding force between the functionalized NPs and the matrixes. To the best of our knowledge, this is the first report on the synthesis of a hierarchical SiO_2/epoxy composite coating without post-treatments like etching or hydrophobization. In this way, a durable superhydrophobic surface with a contact angle of 156° and a sliding angle of 2° is easily created on various substrates. This robust surface maintains the water repellency even after sequential abrasion damages, including finger wiping, brushing, knife scratching, and 600-mesh sandpaper abrasion. It can also endure a 60-kg man standing on its surface for 1 h. More encouragingly, the surface shows an unprecedented thermal stability and it can retain its initial superhydrophobicity even after being exposed directly to fire for 50 s. Superhydrophobic coatings with such an outstanding thermal stability has never been reported before. Moreover, a superior flame-retardant performance of the coated lignocellulosic material is also achieved, manifested by the dramatic improvement in ignition delay (50% delay time in ignition).

2. Materials and methods

2.1. Preparation of superhydrophobic surface

1H, 1H, 2H, 2H-perfluorooctyltrimethoxysilane (F_{13}-TMS) was purchased from Tokyo Chemical Industry, Japan. Silica NPs with a diameter of 15 nm were bought from Shanghai Crystal Pure Biological Technology Co., Ltd., China. Commercial epoxy (E-44) and the curing agents were purchased from Yuanda Chemicals Co., Ltd., China. Chemically pure ethanol was supplied by Tianjin Damao Chemical Reagent Co., Ltd., China. All chemical reagents were used as received without further treatment.

The superhydrophobic surface was prepared as follows. First, 1 g SiO_2 and 0.25 g F_{13}-TMS were dissolved in 20 g ethanol under a strong sonication agitation for 5 min using an ultrasonic cell disruptor (JY 99-IIDN, Ningbo Scientz Biotechnology Co., Ltd., China) operating at 300 W. Then, 2 g epoxy and 1 g curing agent were introduced into the above ethanol dispersion during magnetic stirring for 1.5 h to form a homogeneous reactant solution. Subsequently, the substrate and the reactant solution (1 mL/cm^2) were added into a 25-mL weighting bottle. It was noted that the substrate was fixed at the bottom of the bottle and was completely immersed in the reactant solution. The weighting bottle was then placed into an incompletely sealed vessel. The superhydrophobic surfaces were deposited onto wood, bamboo, and paper after heating the vessel at 110 °C for 1.5 h. For comparison, the reactant solution was spread onto the above substrates with a brush.

2.2. Characterization

The surface morphologies of the as-prepared samples were characterized using a Scanning Electron Microscope (SEM) operated at an accelerating voltage of 10 kV (Hitachi SU1510, Japan). Before SEM examination, all of the samples were sputtered with a thin layer of gold film to improve their conductivity. EDS (Quorum K950X, UK) and FTIR spectroscopy (Shimadzu IRAffinity-1, Japan) were applied to define the surface components of the prepared samples. The water contacting angle (CA) and sliding angle (SA) were measured using a CA measurement device (Data Physics OCA15 Instruments GmbH, Germany). A 4-μL water droplet was used to measure the water CA. The SA was obtained by calculating the CA hysteresis. The difference in the advancing/receding angle was defined as the CA hydrolysis. The advancing angle was measured by gradually pumping water (16 μL) into a small water droplet (4 μL). The receding angle was measured by slowly removing water (16 μL) from the water droplet (20 μL). The durability of the prepared samples was characterized by a series of tests, and the details were described in the Durability Test section in the Supporting Information.

3. Results and discussion

3.1. Fabrication and characterization of the superhydrophobic surfaces

The superhydrophobic surface was directly fabricated on the lignocellulosic substrate with a good mechanical robustness through the thermally-driven method above mentioned (seen route 1 in Fig. 1). Briefly, the SiO_2 NPs, F_{13}-TMS, and epoxy were first dispersed in ethanol by strong sonication agitation to form a homogeneous reactant solution. Then, the lignocellulosic specimen (solid wood) was directly immersed into the reactant solution (at an amount of 1 mL/cm^2), which was kept in an incompletely sealed vessel at 110 °C for 1.5 h. During this process, the solution infilled into the pores of the lignocellulose completely, and meanwhile evaporation of the liquid medium was accomplished. At the initial solution-immersion stage, a large amount of ethanol was preserved in the micropores of the substrate. Simultaneously, the epoxy was deposited onto the substrate prior to SiO_2 NPs did (denoted a pre-deposition effect), because of its higher deposition velocity in ethanol. As a result, the SiO_2 NPs were partially encapsulated into the epoxy layer rather than being completely enclosed into the epoxy layer. As the heating time prolongs, the ethanol preserved in the substrate was gradually evaporated. Impact forces driven from the continuous release of gaseous ethanol acted on the epoxy layer, leaving behind a large amount of micrometer-sized pores on its surface. A typical hierarchical structure comprising exposed SiO_2 NPs and micropores was successfully achieved through this approach.

More importantly, this efficient thermally driven method for fabricating durable superhydrophobic surfaces can be applied to various substrates including wood, bamboo, and filter paper (seen Fig. 2, and Fig. S1 in the Supporting Information). The transverse section of a wood

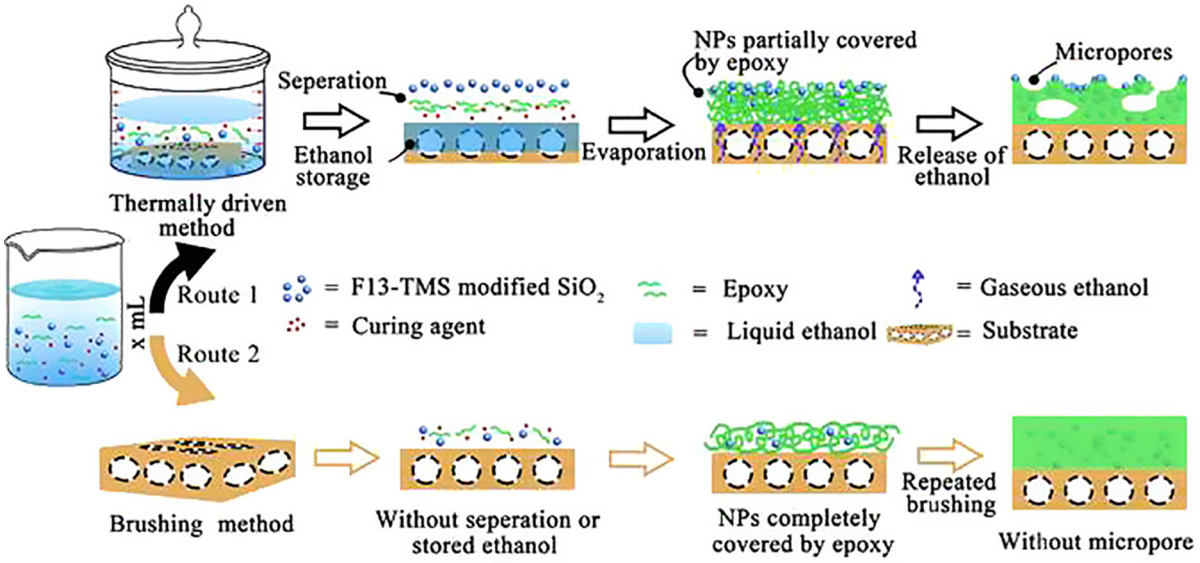

Fig. 1. Schematic illustration of the preparation procedure of SiO_2/epoxy composite coated surfaces.

substrate was tested as a representative for further studies. Scanning electron microscope (SEM) images of the sample prepared using the one-step thermally driven method (denoted as T-treated surface) showed that the T-treated surface was completely covered by the epoxy layer. A substantial amount of micropores with an average size of ~100 μm was observed within the epoxy layer (seen in Fig. 3a).

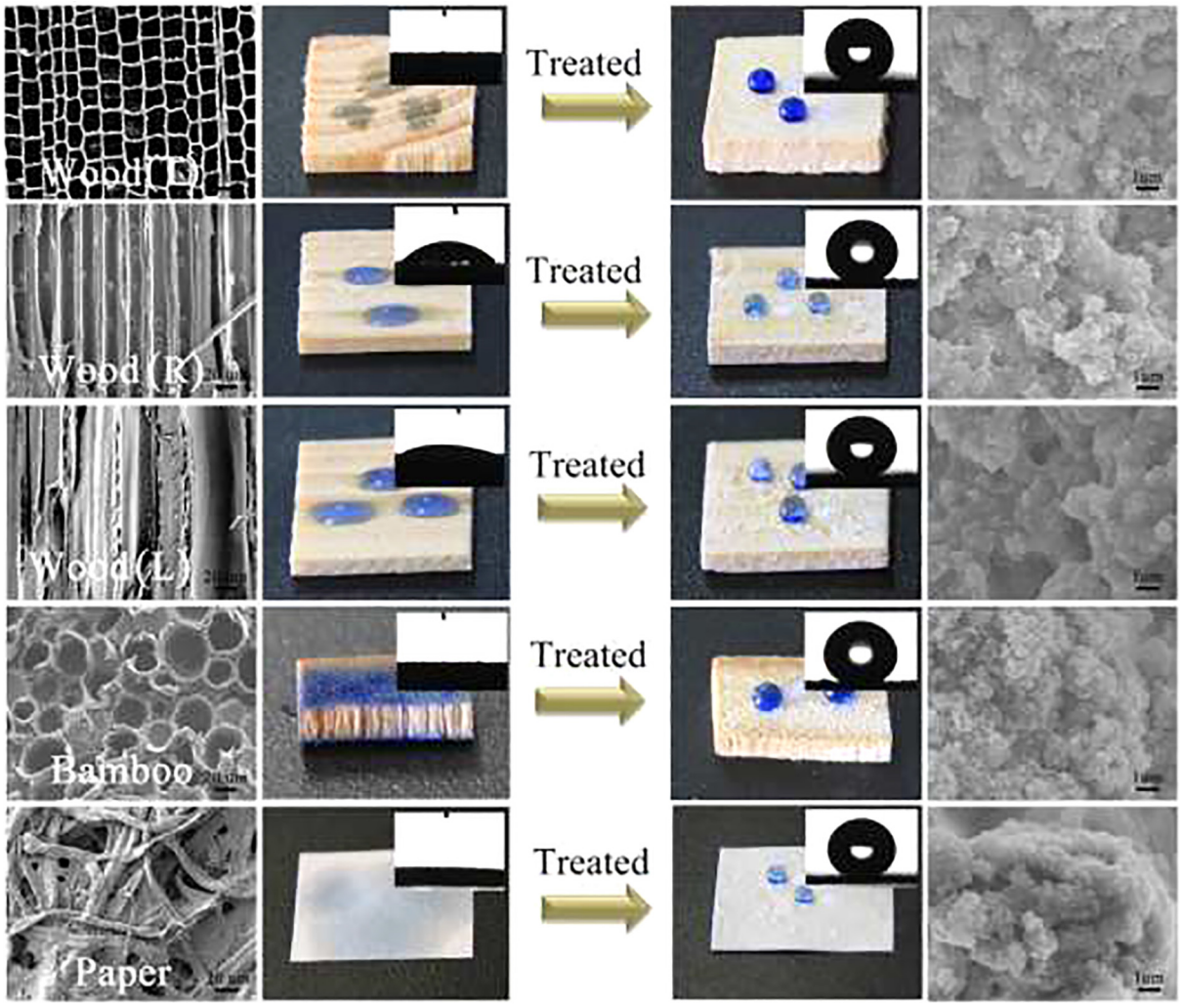

Fig. 2. Surface morphology and wettability of different materials before and after superhydrophobic treatment. Shown in the insets are optical images of the static water droplet (4 μL).

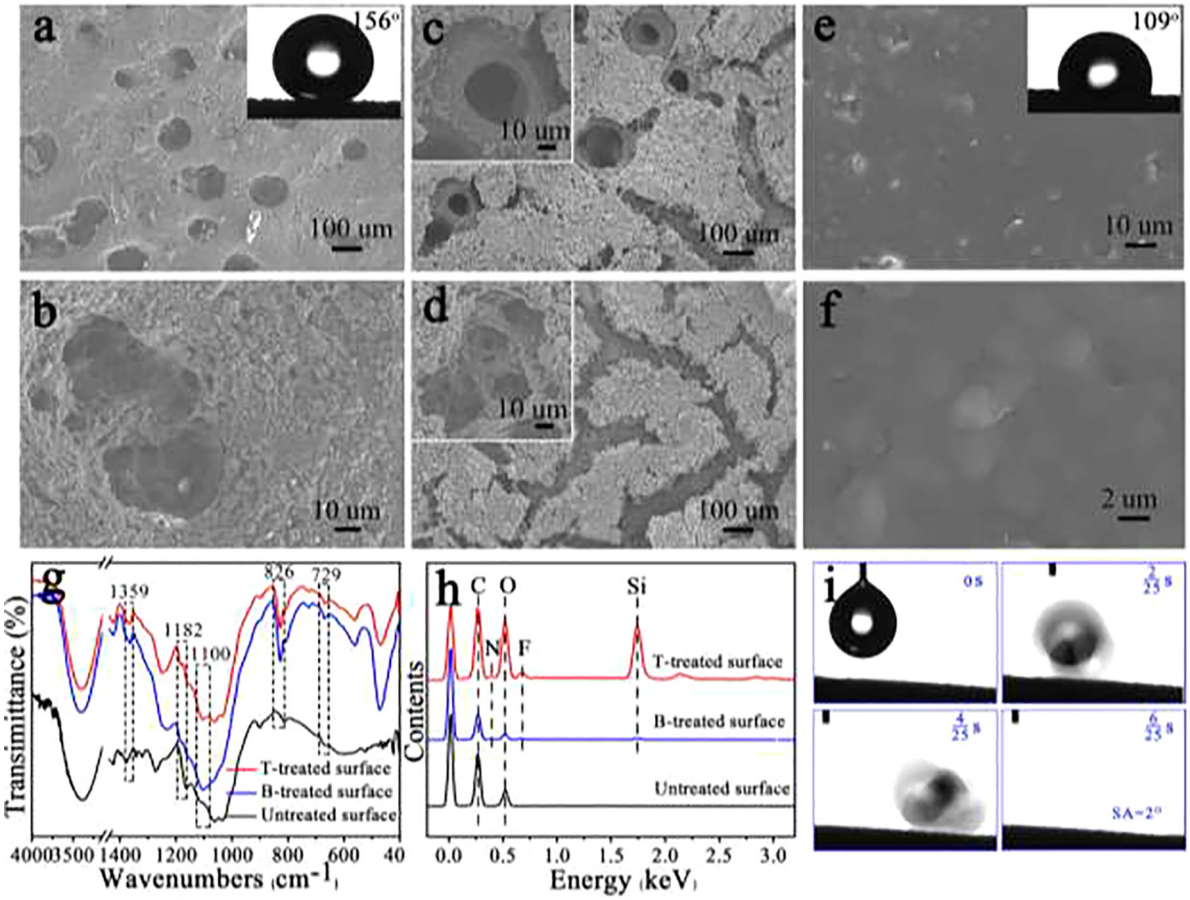

Fig. 3. Characterization of the surfaces coated with SiO_2/epoxy composite (a–d) SEM and magnified images of the T-treated surface (a–c) and B-treated surface (d). The insets in (a, d) showing the corresponding water contact angle. (e–f) The FTIR (e) and EDS (f) spectra of the untreated surface, B-treated surface and T-treated surface. (g) The evolution process of a water droplet (4 μL) sliding away from the T-treated surface.

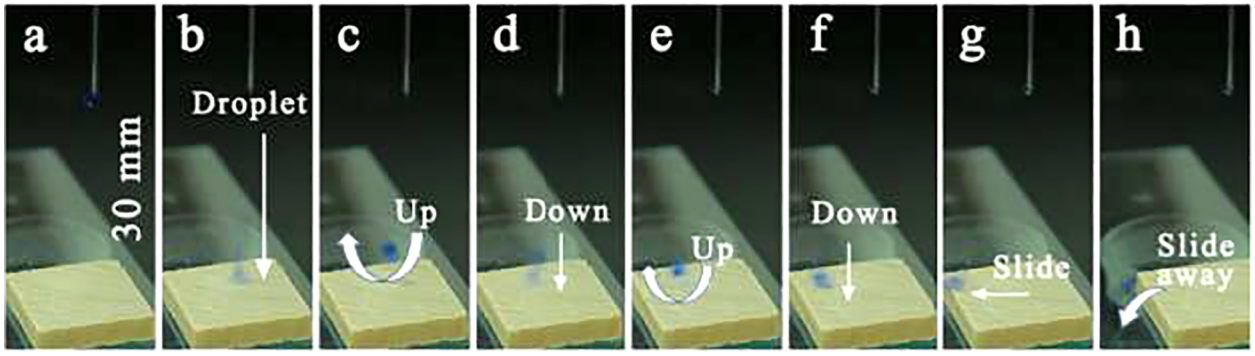

Fig. 4. Time-lapse photographs of water droplet (20 μL) bouncing on superhydrophobic surface.

Moreover, numerous pit-like features formed by the cross-linked epoxy were found inside these pores (seen in Fig. 3b), which increased the surface roughness further. Additionally, dense SiO_2 NPs were found on the epoxy layer surface, appearing as white points, indicating that NPs were partially embedded in epoxy rather than were completely enclosed (seen in Fig. 3b). The partially enclosed SiO_2 NPs verified the pre-deposition effect of the epoxy, in good agreement with the result of cross sectional SEM images of the T-treated surface (seen in Fig. S2 in the Supporting Information). As shown in Fig. S2, micro-scale particulate protrusions consisting of SiO_2 NPs were found on the top layer of the epoxy, while a continuous and smooth epoxy polymer was observed in the middle layer. Further, the pre-deposition effect of epoxy was evidenced by the SEM images of the T-treated surface after removal of the top layer (seen in Fig. 3c–d). Specifically, etching treatment was performed using a torch to remove the top NP layer. SEM image proved that the newly generated morphology around the pores became smoother after the top layer was removed (seen in Fig. 3c). The morphology of the exposed underlying layer far away from the pores demonstrated a highly cross-linked structure (Fig. 3d). The smooth surface and the cross-linked structure were the typical characteristics of epoxy. Therefore, it can be further confirmed that the epoxy layer was deposited beneath the NP layer. The chemical composition of the T-treated surface was subsequently characterized by Fourier-transform infrared (FTIR) spectra and energy-dispersive X-ray spectroscopy (EDS).

The C—F vibration at peaks of 1359, 1182, and 729 cm^{-1} [53–54], Si—O—Si vibration at a peak of 1100 cm^{-1} [55], and epoxy groups at a peak of 826 cm^{-1} [56] confirmed that hydrophobic F_{13}-TMS successfully modified the SiO_2/epoxy composite coating (seen in Fig. 3g), which is consistent with the results of EDS spectra (seen in Fig. 3h, Tables S1–S3 in the Supporting Information). Therefore, it could be concluded that the low surface free energy and interesting architecture of the T-treated surface contributed to an excellent superhydrophobicity. The excellent property of the superhydrophobic surface includes a water contact angle of 156° and a sliding angle of 2° (seen in the inset of Fig. 3a, i, Movie S1 in the Supporting Information), as well as the water droplet bouncing (seen in Fig. 4, Movie S2, Supporting Information), water jetting (seen in Fig. S3, Movie S3, Supporting Information), and self-cleaning performance (seen in Fig. S4, Supporting Information).

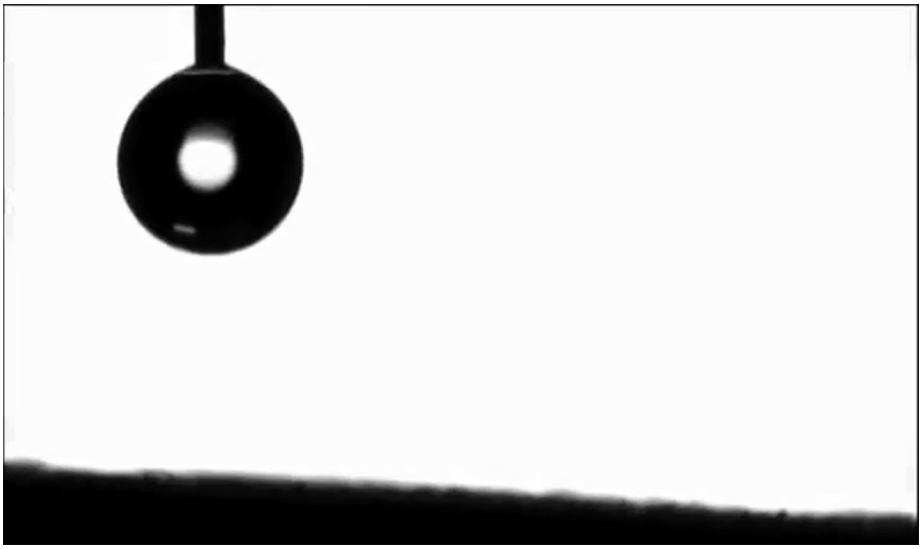

Movie S1.

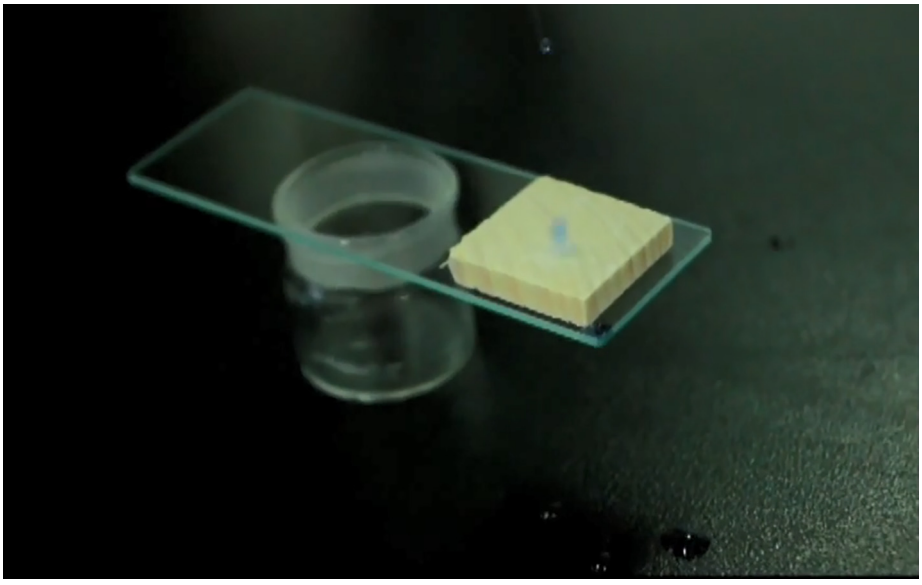

Movie S2.

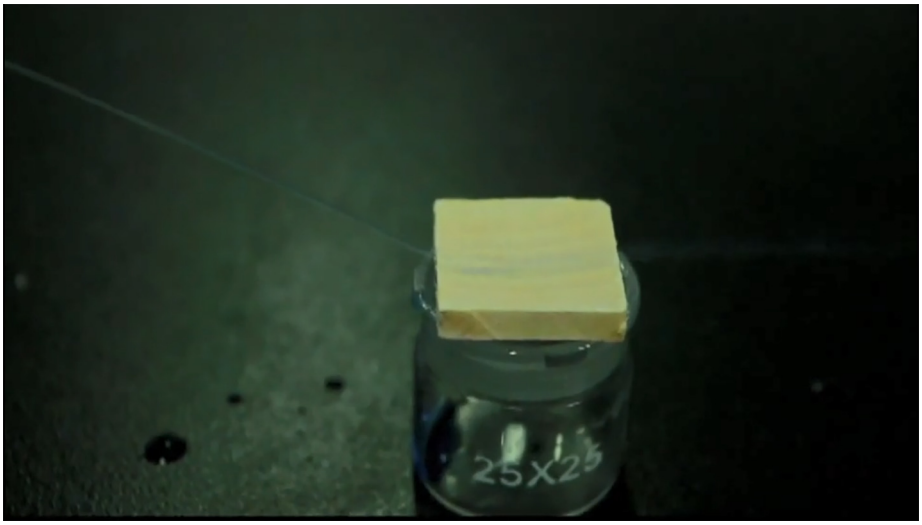

Movie S3.

In contrast, the sample prepared via a conventional brushing method using the same reactant solution (Route 2 in Fig. 1, denoted as the B-treated surface) had a relatively smooth surface with the SiO_2 NPs completely enclosed inside the epoxy layer (Fig. 3e–f). In turn, the B-treated surface only exhibited a much smaller water contact angle of 109° despite with the same chemical composition as the T-treated surface (inset of Fig. 3e, g–h), and failed to achieve superhydrophobicity.

3.2. Durability of the superhydrophobic surfaces in harsh conditions

600-Mesh sandpapers under different pressures were used to rub the superhydrophobic surfaces (see Fig. S5 in the Supporting Information). The results showed that the rubbed surfaces retained their superhydrophobicity, with water CAs of ~150° and SAs of ~10° after a 300 cm abrasion length at the pressure of 2 kPa, 160 cm abrasion length at the pressure of 5 kPa, and 110 cm abrasion length at the pressure of 10 kPa (seen in Fig. 5a–b). SEM images showed that the abraded surface (after a 300 cm abrasion length at the pressure of 2 kPa) retained a hierarchical structure composed of undamaged micropores with a small amount of wear-induced flower-like SiO_2/epoxy coating (seen in Fig. 5c–d). Interestingly, the abraded superhydrophobic coating still remained inside the pores rather than separated from the surface (see Fig. 5e). Moreover, the harsh abrasions had negligible effect on the interior structure of the micropores (Fig. 5f). These results indicated an exceptional interfacial adhesion between the coating and the underneath substrate, which was further confirmed by sequential abrasion tests, including severe finger wiping, repeated brushing, tough knife scratches, and harsh sandpaper abrasion (seen in Fig. 5g, Movie S4 in the Supporting Information). Because these functional coatings are prone to suffer from textural fragility [56,57–58], we further performed a test by standing on the surface. As illustrated in Fig. 5h, a 60-kg person wearing shoes with ridged rubber soles stood on the superhydrophobic wood surface with the shoes in full contact with the tested wood sample (a typical pressure of 474 kPa). After standing on the surface for 1 h, the superhydrophobicity was not influenced. The surface maintained a good water repellency, as indicated by a CA of 151°, spherical water droplets, and rough structure without crushing scars. This superior mechanical stability is benefited from the epoxy layer within the micrometer-sized pores, which functions as a soft binder to anchor the coating and as a stress relief layer to release the applied force. The remarkable characteristics make the obtained superhydrophobic material has great potentials in applications such as flooring.

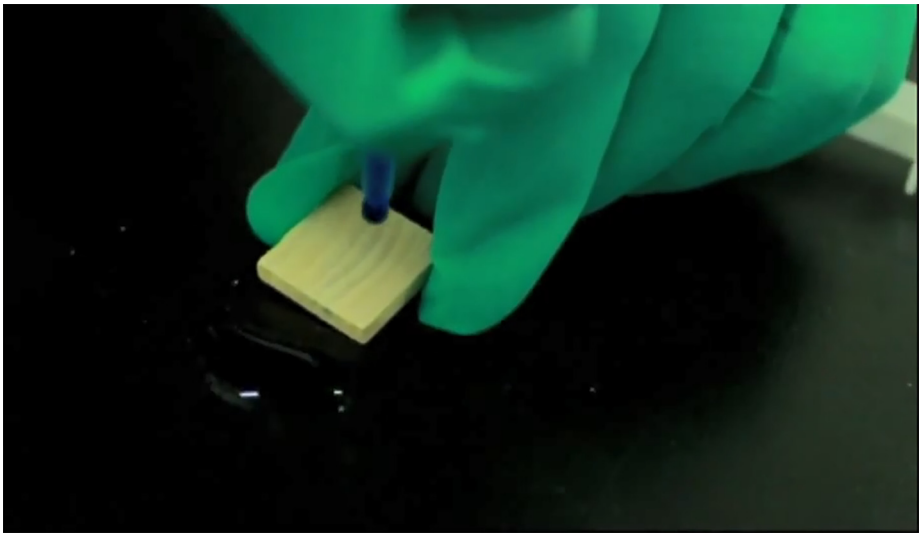

Movie S4.

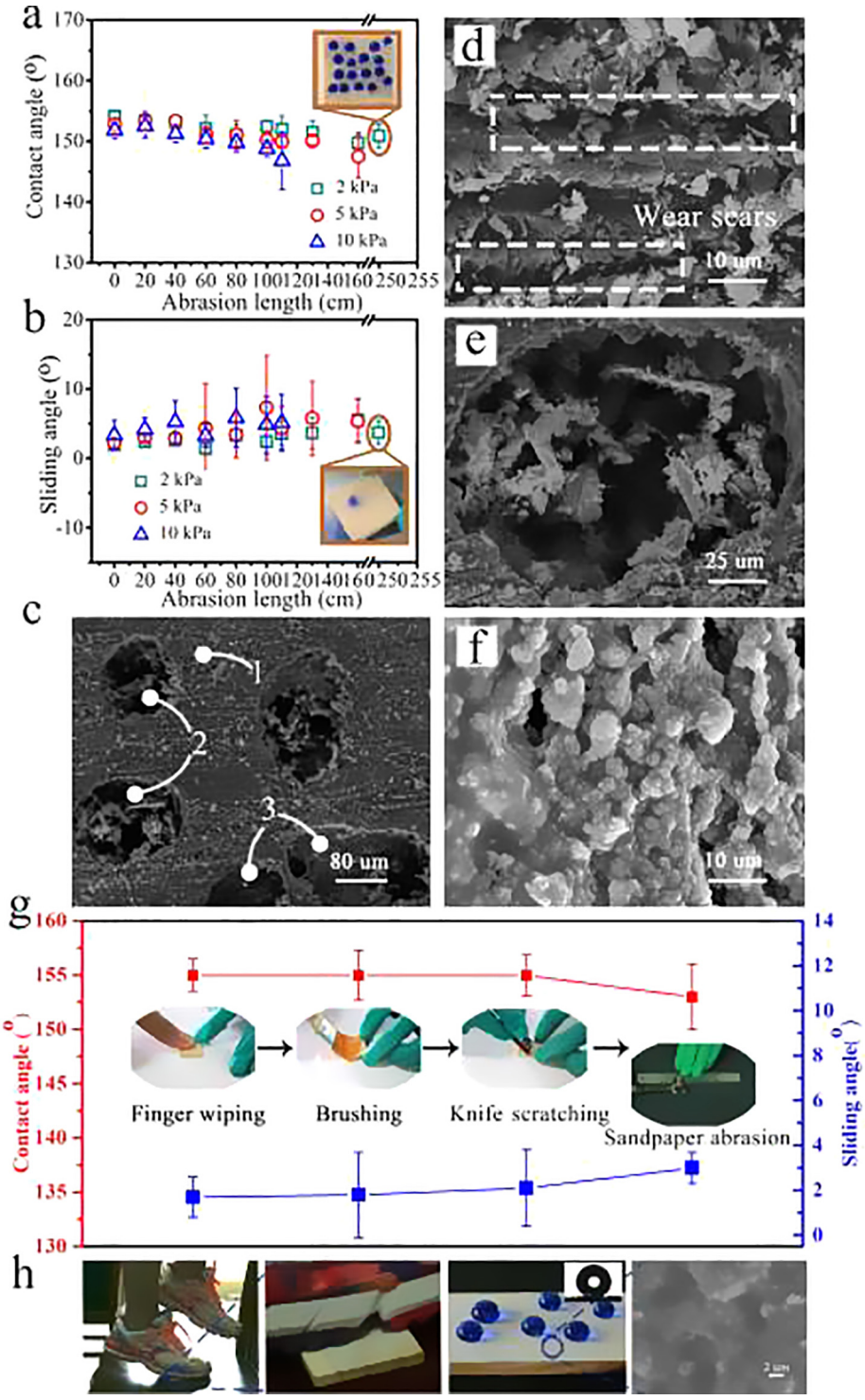

Fig. 5. Mechanical stability characterization of the prepared superhydrophobic surface. a, b) Abrasion length-dependent contact angles (a) and sliding angles (b) of the superhydrophobic surface rubbed with different pressures. (c–f) SEM characterization of the abraded surface. Note that (d–f) correspond to the marked 1, 2, 3 areas, respectively. (g) Changes in contact angles and sliding angles during a sequential abrasion damage, including finger wiping, brushing, knife scratching, and sandpaper abrasion. (h) Change in water repellency and microstructure of the superhydrophobic wood after a 60 kg man stood on its surface for 1 h.

Aside from the outstanding mechanical stability, the prepared superhydrophobic surfaces also exhibited high chemical stability. Their superhydrophobic property was maintained after immersion into aqueous solutions with pH values ranged from 1 to 13 for 1 h (seen in Fig. S6, Supporting Information). A self-designed spray gun with tunable pressure was used to test their acid/alkaline-rain corrosion resistance in a

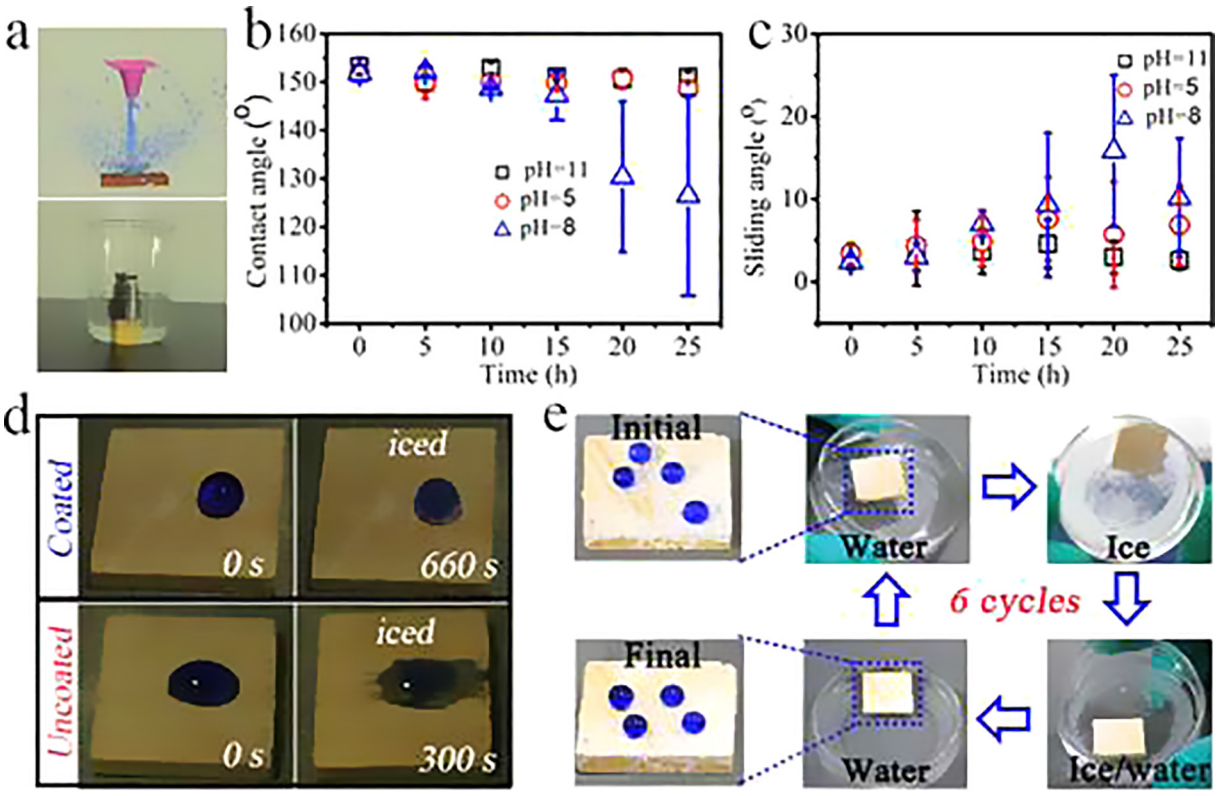

Fig. 6. Chemical stability of the prepared superhydrophobic surface and their performance in harsh environmental condition. (a) Schematic illustration of heavy corrosive rain impact test and sea water corrosion test. (b, c) Time-dependent contact angles (b) and sliding angles (c) of the superhydrophobic surface after acid/alkaline rain and sea water corrosion. (d) Anti-icing test. (e) Freeze-thaw test.

realistic rainfall scenario (seen in Fig. 6a). The superhydrophobic wood could sustain heavy acid/alkali rain for 25 h without water-repellent performance degradation (see Fig. 6b–c). Additionally, it could endure seawater corrosion for 15 h (at pH = 8), demonstrating great promise for maritime applications. The superhydrophobic surface also exhibited superior anti-icing performance. The freezing time of a 40-μL water droplet on the superhydrophobic surface was delayed to 660 s (in contrast with 330 s for an untreated surface; see Fig. 6d). The superhydrophobic performance in a complex ice/water environment was investigated by a freeze-thaw test according to a previous literature [59]. As expected, the wood had almost no deformation and could support spherical water droplets on its surface after six freeze-thaw cycles (see Fig. 6e), with more details given in the Supporting Information. All of these properties significantly enhance the long-term durability of the coatings and make it suitable for a wide range of practical applications.

3.3. Stability of the superhydrophobic surfaces exposed to high-temperature flame

The stability of the superhydrophobic coatings at high temperature is important for practical applications, especially for lignocellulose-based materials that are readily degradation under high temperatures. For superhydrophobic lignocellulose-based materials, superhydrophobic stability at high temperatures is related to flame retardancy, owing to the fact that such property can enhance the resistance towards deformation of both substrates and coatings. The flame retardancy was evaluated by comparing the combustion behaviours of untreated and the superhydrophobic wood in a real flame. The details of the process were illustrated in Fig. 7. Both samples were exposed to a direct flame (> 500 °C) provided by a torch. The fire source was withdrawn after the samples were ignited. The untreated wood ignited after 4 s exposure (see Fig. 7a). The flame spread rapidly and became increasingly bright even after removing the fire source. After 20 s combustion, the wood surface was entirely covered by flame. However, the combustion process of the superhydrophobic wood differed dramatically from that of the untreated sample (see Fig. 7b). The flame on the treated surface was still weak after 4 s exposure, and only a few black burn marks were found over a small area. Its ignition duration was delayed to 6 s, approximately 1.5 times longer than that of the untreated wood. Moreover, it took 50 s for the surface to be entirely covered by flame, 2.5 times longer than the untreated one. There were three major differences displayed between these two kinds of samples, including shape, strength, and completeness of combustion. The deformation of the untreated wood after burn-out was more obvious than that of the superhydrophobic wood. In contrast, the untreated wood had a very weak strength because it could be crushed by even slight finger touch (see Fig. S7, Supporting Information). However, the superhydrophobic wood could sustain finger pressing without breaking (see Fig. S7, Supporting Information). Finally, the completeness of combustion was 85.8% for the superhydrophobic wood, whereas it was 96% for the untreated wood, as determined by calculating the weight

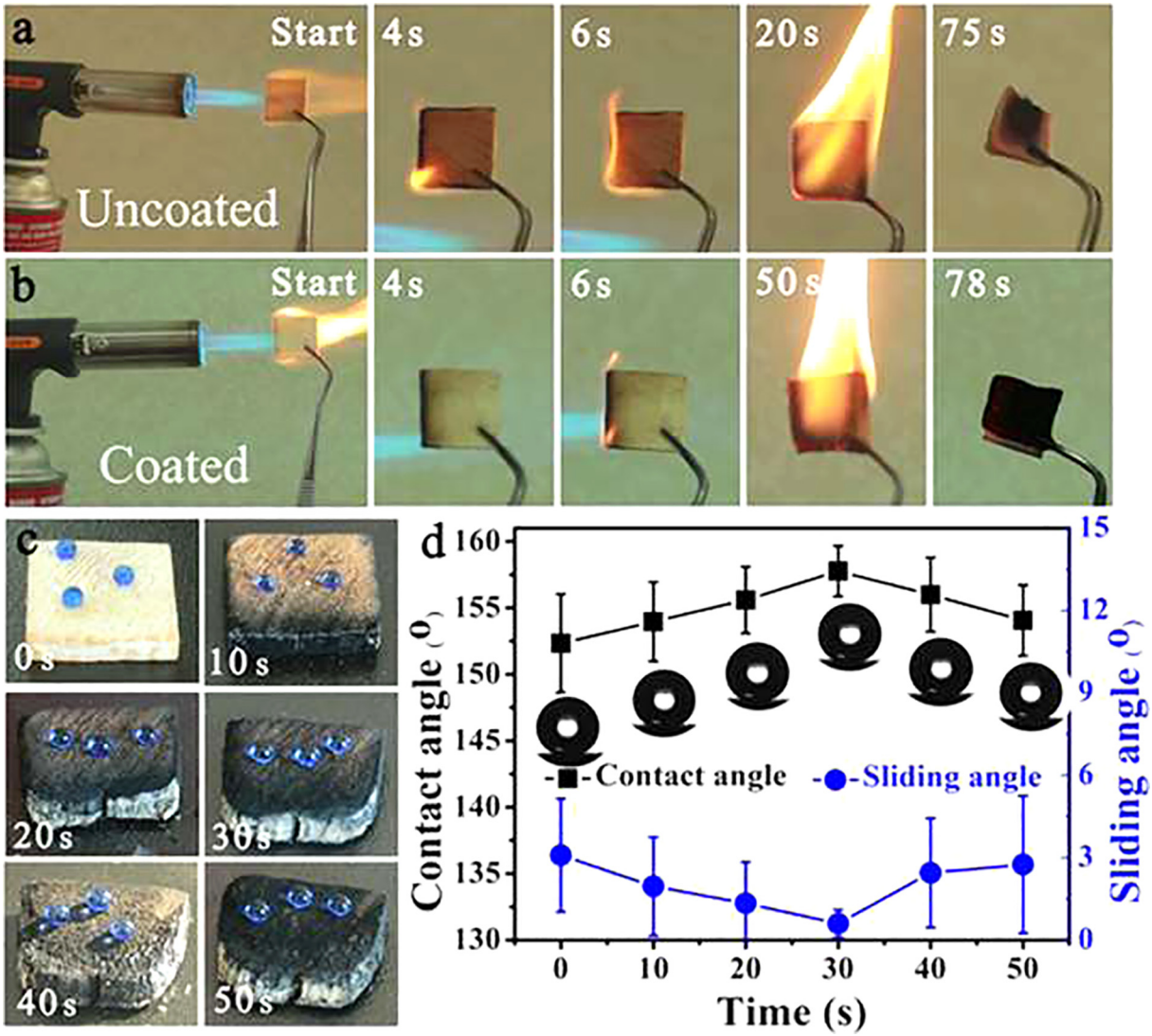

Fig. 7. Stability of the superhydrophobic surface exposed to fire. (a, b) The combustion process of the untreated wood (a) and superhydrophobic wood (b). (c) Water droplets standing on the superhydrophobic wood surface after it was exposed to fire. (d) The contact angle and sliding angle of the resultant wood surface as a function of exposure time to fire.

ratio between the wood sample before and after burn-out.

The water-repellent performance of the superhydrophobic wood surface was recorded every 10 s during the combustion process. As illustrated in Fig. 7c, the black burn marks gradually became darker and spread across the entire surface. However, spherical water droplets were still well supported by the resulting surface rather than absorbed, which has rarely been reported. Notably, the resulting surface had a larger CA value and a lower SA value than before (see Fig. 7d), which can be attributed to its improved roughness after exposure to fire (see Fig. 3c–d). All of these observations prove that the superhydrophobic coating offers strong fire retardancy and remarkable superhydrophobic stability at extremely high temperatures, which would definitely widen the application fields of the superhydrophobic materials [60–61].

We further evaluated the thermal stability of the superhydrophobic surface at several constant temperatures including 100 °C, 200 °C, and 300 °C. The results demonstrated that the resultant surfaces still had high contact angles of ~155° and lower water adhesion after being heated at 100 °C for 264 h, at 200 °C for 156 h, and at 300 °C for 14 h, respectively (see Fig. 8, Movie S5 in the Supporting Information). It could be also found that the CAs of the resultant surfaces were higher than its original state, in good agreement with the result of combustion test. These results confirm the excellent thermal stability of the superhydrophobic surfaces. It is necessary to illustrate that 264 h and 156 h are not the maximum times that the superhydrophobic surfaces can withstand without the loss of superhydrophobicity when have been heated at 100 °C and 200 °C, respectively. The inset pictures of Fig. 8 showed that the spherical water droplets could be supported by the surfaces before and after thermal stability tests, even though the substrate material deformed because of thermal degradation, further indicating the excellent thermal stability and mechanical stability.

Movie S5.

The thermal properties of the superhydrophobic surfaces and the untreated surfaces were also assessed by TG test. As shown in Fig. S8, the untreated surface with a loss of 82.31% of the initial weight with one major decomposition step in the temperature range of 200–600 °C. The maximum mass loss rate appeared at 369 °C. In terms of superhydrophobic surfaces, a major step of degradation occurred in the temperature range of 300–500 °C with a weight loss of 75.86% compared to the initial weight. The maximum mass loss rate appeared at 399 °C. It could be confirmed that the surface after superhydrophobic treatment exhibited enhanced thermal stability, featured by the delayed temperature where reaches the maximum mass loss rate, the decreased weight loss, as well as the narrowed temperature range of decomposition.

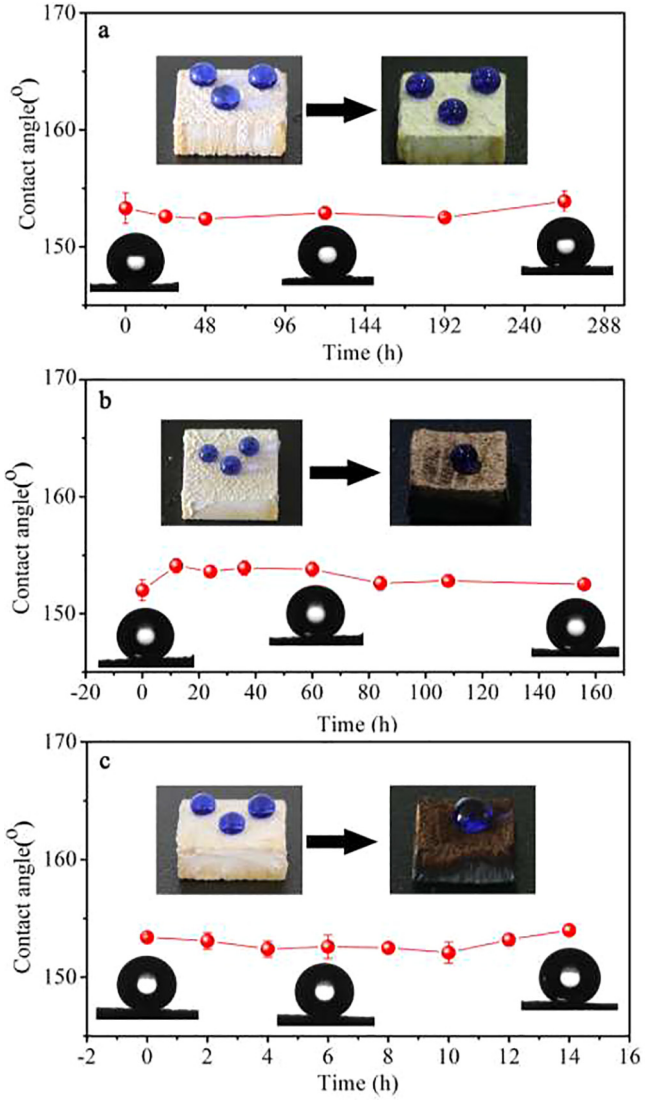

Fig. 8. The changes in CA of the superhydrophobic surfaces after having been heated for a long time at different temperatures: (a) 100 °C, (b) 200 °C, (3) 300 °C.

4. Conclusions

In summary, we fabricated a hierarchically structured epoxy layer with durable superhydrophobic surfaces via an efficient one-step thermally driven method. In contrast to most traditional strategies, the epoxy served not only as a soft binder and stress-buffer layer to boost robustness, but also provided microscale roughness to support superhydrophobicity. Because of the different settling velocity of epoxy and SiO_2 NPs in ethanol, the epoxy layer was deposited beneath the NP layer. In this way, the top NPs were partially encapsulated on the epoxy layer rather than were completely enclosed, giving rise to nanoscale roughness of the epoxy layer. The evaporation of the ethanol preserved in the substrate induced impact force on the epoxy layer, leaving behind a large number of pores with an average size of ~100 μm, endowing microscale roughness to the epoxy layer. The as-prepared surfaces exhibited superhydrophobicity with a CA of 156° and a SA of 2°. Moreover, the functional surfaces were able to endure sequential abrasion damage, including severe finger wiping, repeated brushing, harsh knife scratching, and tough 600-mesh sandpaper abrasion. Additionally, the surfaces could withstand a 60-kg man standing on it for 1 h without influencing its original performance. It was also found that the superhydrophobic surfaces exhibited outstanding anti-icing, anti-fire, anti-corrosion properties, as well as thermal stability. In particular, it could maintain superhydrophobicity even after combustion for 50 s. The facile one-step processing route rendered superhydrophobic surfaces with excellent durability and remarkable stability when exposed to fire will have practical applications in a wide range of fields.

Acknowledgments

This work was financially supported by the National Natural Science Foundation of China (31270602), Key Laboratory of Bio-based Material Science & Technology, Ministry of Education (SWZCL2016-02), Young Elite Scientists Sponsorship Program by CAST (2016QNRC001), Outstanding Innovative Youth Training Program of Changsha

(KQ1707019), and Hunan Provincial Technical Innovation Platform and Talent Program in Science and Technology (2016RS2010, 2016TP1013).

Appendix A. Supplementary data

Supplementary data associated with this article can be found, in the online version, at http://dx.doi.org/10.1016/j.cej.2018.04.195.

References

[1] E. Chiellini, R. Solaro, Biodegradable polymeric materials, Adv. Mater. 8 (1996) 305–313.
[2] D. Klemm, B. Heublein, H.P. Fink, A. Bohn, Cellulose, chemistry and application, Angew. Chem. Int. Ed. 44 (2005) 3358–3393.
[3] J.B. Binder, R.T. Raines, Simple chemical transformation of lignocellulosic biomass into furans for fuels and chemicals, J. Am. Chem. Soc. 131 (2009) 1979–1985.
[4] D.W. Zhao, C.J. Chen, Q. Zhang, W.S. Chen, S.X. Liu, Q.W. Wang, Y.X. Liu, J. Li, H.P. Yu, High performance, flexible, solid-state supercapacitors based on a renewable and biodegradable mesoporous cellulose membrane, Adv. Energy Mater. (2017) 1700739.
[5] F.F. Chen, Y.J. Zhu, Z.C. Xiong, T.W. Sun, Y.Q. Shen, Highly flexible superhydrophobic and fire-resistant layered inorganic paper, ACS. Appl. Mater. Interfaces 8 (2016) 34715–34724.
[6] B. Guo, Y. Liu, Q. Zhang, F. Wang, Q. Wang, Y. Liu, J. Li, H. Yu, Efficient flame-retardant and smoke-suppression properties of Mg-Al-layered double-hydroxide nanostructures on wood substrate, ACS. Appl. Mater. Interfaces 9 (2017) 23039–23047.
[7] C. Ruan, K. Ai, X. Li, L. Lu, A superhydrophobic sponge with excellent absorbency and flame retardancy, Angew. Chem. Int. Ed. 53 (2014) 5556–5560.
[8] W. Barthlott, C. Neinhuis, Purity of the sacred lotus, or escape from contamination in biological surfaces, Planta (1997) 1–8.
[9] J. Li, L. Yan, X. Tang, H.T. Feng, D. Hu, F. Zha, Robust superhydrophobic fabric bag filled with polyurethane sponges used for vacuum-assisted continuous and ultrafast absorption and collection of oils from water, Adv. Mater. Interfaces 3 (2016) 1500770.
[10] R. Wang, K. Hashimoto, A. Fujishima, M. Chikuni, E. Kojima, A. Kitamura, M. Shimohigoshi, T. Watanabe, Light-induced amphiphilic surfaces, Nature 388 (1997) 431–432.
[11] X.M. Li, D. Reinhoudt, M.C. Calama, What do we need for a superhydrophobic surface? A review on the recent progress in the preparation of superhydrophobic surfaces, Chem. Soc. Rev. 36 (2007) 1350–1368.
[12] Z.Q. Sun, T. Liao, K.S. Liu, L. Jiang, J. Kim, S.X. Dou, Robust superhydrophobicity of hierarchical ZnO hollow microspheres fabricated by two-step self-assembly, Nano Res. 6 (2013) 726–735.
[13] K. Liu, X. Yao, L. Jiang, Recent developments in bio-inspired special wettability, Soc. Rev. 39 (2010) 3240–3255.
[14] S. Huang, J.L. Song, Y. Lu, F.Z. Chen, H.X. Zheng, X.L. Yang, X. Liu, J. Sun, C.G. Carmalt, I.P. Parkin, W.J. Xu, Underwater spontaneous pumpless transportation of nonpolar organic liquids on extreme wettability patterns, ACS. Appl. Mater. Interfaces 8 (2016) 2942–2949.
[15] W. Barthlott, T. Schimmel, S. Wiersch, K. Koch, M. Brede, M. Barczewski, S. Walheim, A. Weis, A. Kaltenmaier, A. Leder, H.F. Bohn, The Salvinia paradox: superhydrophobic surfaces with hydrophilic pins for air retention under water, Adv. Mater. 22 (2010) 2325–2328.
[16] J. Li, C.C. Xu, Y. Zhang, R.F. Wang, F. Zha, H.D. She, Robust superhydrophobic attapulgite coated polyurethane sponge for efficient immiscible oil/water mixture and emulsion separation, J. Mater. Chem. A 4 (2016) 15546–15553.
[17] J. Li, D. Li, Y. Yang, J. Li, F. Zha, Z. Lei, A prewetting induced underwater superoleophobic or underoil (super) hydrophobic waste potato residue-coated mesh for selective efficient oil/water separation, Green Chem. 18 (2016) 541–549.
[18] J.L. Song, S. Huang, Y. Lu, X.W. Bu, J.E. Mates, A. Ghosh, R. Ganguly, C.G. Carmalt, I.P. Parkin, W.J. Xu, C.M. Megaridis, Self-driven one-step oil removal from oil spill on water via selective-wettability steel mesh, ACS. Appl. Mater. Interfaces 6 (2014) 19858–19865.
[19] J. Li, L. Yan, H. Li, W. Li, F. Zha, Z. Lei, Underwater superoleophobic palygorskite coated meshes for efficient oil/water separation, J. Mater. Chem. A 3 (2015) 14696–14702.
[20] R. Chen, M.C. Lu, V. Srinivasan, Z. Wang, H.H. Cho, A. Majumdar, Nanowires for enhanced boiling heat transfer, Nano. Lett. 9 (2009) 548–553.
[21] A.M. Emelyanenko, L.B. Boinovich, A.A. Bezdomnikov, E.V. Chulkova, K.A. Emelyanenko, Reinforced superhydrophobic coating on silicone rubber for longstanding anti-icing performance in severe conditions, ACS. Appl. Mater. Interfaces 9 (2017) 24210–24219.
[22] Y. Li, D.X. Luong, J. Zhang, Y.R. Tarkunde, C. Kittrell, F. Sargunaraj, Y. Ji, C.J. Arnusch, J.M. Tour, Laser-induced graphene in controlled atmospheres: from superhydrophilic to superhydrophobic surfaces, Adv. Mater. 29 (2017) 1700496.
[23] J.L. Zhang, C.G. Gu, J.P. Tu, Robust slippery coating with superior corrosion resistance and anti-icing performance for AZ31B Mg alloy protection, ACS. Appl. Mater. Interfaces 9 (2017) 11247–11257.
[24] M. He, Q.L. Zhang, X.P. Zeng, D.P. Cui, J. Chen, H.L. Li, J.J. Wang, Y.L. Song, Hierarchical porous surface for efficiently controlling microdroplets' self-removal, Adv. Mater. 25 (2013) 2291–2295.
[25] K.K. Varanasi, T. Deng, J.D. Smith, M. Hsu, N. Bhate, Frost formation and ice adhesion on superhydrophobic surfaces, Appl. Phys. Lett. 97 (2010) 234102.
[26] Y.J. Zhu, F.L. Sun, H.J. Qian, H.Y. Wang, L.W. Mu, J.H. Zhu, A biomimetic spherical cactus superhydrophobic coating with durable and multiple anti-corrosion effects, Chem. Eng. J. 338 (2018) 670–679.
[27] Z.Q. Sun, T. Liao, K.S. Liu, L. Jiang, J.H. Kim, S.X. Dou, Fly-eye inspired superhydrophobic anti-fogging inorganic nanostructures, Small 10 (2014) 3001–3006.
[28] Y.S. Li, H. Shao, P.F. Lv, C.Y. Tang, Z.K. He, Y.L. Zhou, M.B. Shuai, J. Mei, W.M. Lau, Fast preparation of mechanically stable superhydrophobic surface by UV cross-linking of coating onto oxygen-inhibited layer of substrate, Chem. Eng. J. 338 (2018) 440–449.
[29] J. Ju, X. Yao, X. Hou, Q.H. Liu, Y.S. Zhang, A. Khademhosseini, A highly stretchable and robust non-fluorinated superhydrophobic surface, J. Mater. Chem. A 5 (2017) 16273–16280.
[30] X.L. Tian, T. Verho, R.H.A. Ras, Moving superhydrophobic surfaces toward real-world applications, Science 352 (2016) 142–143.
[31] X.J. Guo, C.H. Xue, S.T. Jia, J.Z. Ma, Mechanically durable superamphiphobic surfaces via synergistic hydrophobization and fluorination, Chem. Eng. J. 320 (2017) 330–341.
[32] J. Li, Z.H. Zhao, R.M. Kang, Y. Zhang, W.Z. Lv, M.J. Li, R.N. Jia, L.J. Luo, Robust superhydrophobic candle soot and silica composite sponges for efficient oil/water separation in corrosive and hot water, J. Sol-Gel. Sci. Technol. 82 (2017) 817–826.
[33] X. Huang, X. Kong, Y.W. Cui, X.X. Ye, X.L. Wang, B. Shi, Durable superhydrophobic materials enabled by abrasion-triggered roughness regeneration, Chem. Eng. J. 336 (2018) 633–639.
[34] Y. Lu, S. Sathasivam, J.L. Song, C.R. Crick, C.J. Carmalt, I.P. Parkin, Robust self-cleaning surfaces that function when exposed to either air or oil, Science 347 (2015) 1132–1135.
[35] S. Chen, X. Li, Y. Li, J. Sun, Intumescent flame-retardant and self-healing superhydrophobic coatings on cotton fabric, ACS Nano 9 (2015) 4070–4076.
[36] X.C. Tian, S. Shaw, K.R. Lind, L. Cademartiri, Thermal processing of silicones for green, scalable, and healable superhydrophobic coatings, Adv. Mater. 28 (2016) 3677–3682.
[37] M. Wu, Y. Li, N. An, J. Sun, Applied voltage and near-infrared light enable healing of superhydrophobicity loss caused by severe scratches in conductive superhydrophobic films, Adv. Funct. Mater. 26 (2016) 6777–6784.
[38] H. Zhou, H. Wang, H. Niu, Y. Zhao, Z. Xu, T.A. Lin, Waterborne coating system for preparing robust, self-healing, superamphiphobic surfaces, Adv. Funct. Mater. 27 (2017) 1604261.
[39] L. Zhang, B. Tang, J. Wu, R. Li, P. Wang, Hydrophobic light-to-heat conversion membranes with self-healing ability for interfacial solar heating, Adv. Mater. 27 (2015) 4889–4894.
[40] H. Zhang, C.P. Hou, L.X. Song, Y. Ma, Z. Ali, J.W. Gu, B.L. Zhang, H.P. Zhang, Q.Y. Zhang, A stable 3D sol-gel network with dangling fluoroalkyl chains and rapid self-healing ability as a long-lived superhydrophobic fabric coating, Chem. Eng. J. 334 (2018) 598–610.
[41] M. Wu, B. Ma, T. Pan, S. Chen, J. Sun, Silver-nanoparticle-colored cotton fabrics with tunable colors and durable antibacterial and self-healing superhydrophobic properties, Adv. Funct. Mater. 26 (2016) 569–576.
[42] C. Cao, M. Ge, J. Huang, S. Li, S. Deng, S. Zhang, Z. Chen, K. Zhang, S.S. Al-Deyabd, Y. Lai, Robust fluorine-free superhydrophobic PDMS–ormosil@ fabrics for highly effective self-cleaning and efficient oil–water separation, J. Mater. Chem. A 4 (2016) 12179–12187.
[43] M.J. Nine, M.A. Cole, L. Johnson, D.N.H. Tran, D. Losic, Robust superhydrophobic graphene-based composite coatings with self-cleaning and corrosion barrier properties, ACS. Appl. Mater. Interfaces 7 (2015) 28482–28493.
[44] B. Chen, J. Qiu, E. Sakai, N. Kanazawa, R. Liang, H. Feng, Robust and superhydrophobic surface modification by a "Paint+ Adhesive" method: applications in self-cleaning after oil contamination and oil–water separation, ACS. Appl. Mater. Interfaces 8 (2016) 17659–17667.
[45] Y. Si, Z. Guo, W.A. Liu, Robust epoxy resins@ stearic acid-Mg(OH)$_2$ micronanosheet superhydrophobic omnipotent protective coating for real-life applications, ACS. Appl. Mater. Interfaces 8 (2016) 16511–16520.
[46] L. Chen, Z. Guo, W. Liu, Biomimetic multi-functional superamphiphobic FOTS-TiO$_2$ particles beyond lotus leaf, ACS. Appl. Mater. Interfaces 8 (2016) 27188–27198.
[47] M. Wen, J. Zhong, S.J. Zhao, T.L. Bu, L. Guo, Z.L. Ku, Y. Peng, F.Z. Huang, Y.B. Cheng, Q. Zhang, Robust transparent superamphiphobic coatings on non-fabric flat substrates with inorganic adhesive titania bonded silica, J. Mater. Chem. A 5 (2017) 8352–8359.
[48] M.Y. Long, S. Peng, W.S. Deng, X.R. Miao, N. Wen, Q.N. Zhou, X.J. Yang, W.L. Deng, Robust superhydrophobic PDMS@ZnSn(OH)$_6$ coating with under-oil self-cleaning and flame retardancy, J. Mater. Chem. A 5 (2017) 22761–22771.
[49] Q. Wang, J. Bai, B. Dai, Z.H. Yang, S. Guo, L. Yang, Y.R. He, J.C. Han, J.Q. Zhu, Robust superhydrophobic diamond microspheres for no-loss transport of corrosive liquid microdroplets, Chem. Commun. 53 (2017) 2355–2358.
[50] Y.H. Xiu, Y. Liu, B. Balu, D.W. Hess, C.P. Wong, Robust superhydrophobic surfaces prepared with epoxy resin and silica nanoparticles, IEEE Trans. Comp. Pack. Man. 2 (2012) 395–401.
[51] X. Zhang, Y.F. Si, J.L. Mo, Z.G. Guo, Robust micro-nanoscale flowerlike ZnO/epoxy resin superhydrophobic coating with rapid healing ability, Chem. Eng. J. 313 (2017) 1152–1159.
[52] Y. Liu, Z.Y. Lin, K.S. Moon, C.P. Wong, Reversible superhydrophobic–superhydrophilic transition of ZnO nanorod/epoxy composite films, ACS. Appl. Mater. Interfaces 4 (2012) 3959–3964.
[53] L.K. Gao, Y. Lu, J. Li, Q.F. Sun, Superhydrophobic conductive wood with oil repellency obtained by coating with silver nanoparticles modified by fluoroalkyl silane, Holzforschung 70 (2016) 63–68.
[54] N. Saleema, D.K. Sarkar, D. Gallant, R.W. Paynter, X.G. Chen, Chemical nature of superhydrophobic aluminum alloy surfaces produced via a one-step process using fluoroalkyl-silane in a base medium, ACS. Appl. Mater. Interfaces 3 (2011) 4775–4781.
[55] J.K. Hong, H.R. Kim, H.H. Park, The effect of sol viscosity on the sol–gel derived low density SiO$_2$ xerogel film for intermetal dielectric application, Thin Solid Films 332

(1998) 449–454.
[56] Y.Q. Wu, S.S. Jia, S. Wang, Y. Qing, N. Yan, Q.H. Wang, T.T. Meng, A facile and novel emulsion for efficient and convenient fabrication of durable superhydrophobic materials, Chem. Eng. J. (2017), http://dx.doi.org/10.1016/j.cej.2017.07.023.
[57] Y.Q. Wu, S.S. Jia, Y. Qing, S. Luo, M. Liu, A versatile and efficient method to fabricate durable superhydrophobic surfaces on wood, lignocellulosic fiber, glass, and metal substrates, J. Mater. Chem. A 4 (2016) 14111–14121.
[58] W.B. Zhang, T.H. Xiang, F. Liu, M. Zhang, W.T. Gan, X.L. Zhai, X. Di, Y.Z. Wang, G.X. Liu, C.Y. Wang, Facile design and fabrication of superwetting surfaces with excellent wear-resistance, ACS. Appl. Mater. Interfaces 9 (2017) 15776–15784.
[59] J.L. Song, D.Y. Zhao, Z.J. Han, W. Xu, Y. Lu, X. Liu, B. Liu, C.J. Carmalt, X. Deng, I.P. Parkin, Super-robust superhydrophobic concrete, J. Mater. Chem. A 5 (2017) 14542–14550.
[60] F.F. Chen, Y.J. Zhu, Z.C. Xiong, L.Y. Dong, F. Chen, B.Q. Lu, R.L. Yang, Hydroxyapatite nanowire-based all-weather flexible electrically conductive paper with superhydrophobic and flame-retardant properties, ACS. Appl. Mater. Interfaces 9 (45) (2017) 39534–39548.
[61] R.L. Yang, Y.J. Zhu, F.F. Chen, L.Y. Dong, Z.C. Xiong, Luminescent, fire-resistant, and water-proof ultralong hydroxyapatite nanowire-based paper for multimode anticounterfeiting applications, ACS Appl. Mater. Interfaces 9 (30) (2017) 25455–25464.